ingegneria sismica
International Journal of Earthquake Engineering
Anno XLIII - Num. 2 - 2026

Hierarchical Control Algorithms for Integrated PV–Storage–Charging Systems with Grid-Forming Energy Storage

Tengchang Li[1,*], *Yuzhang Xu*[1] *and Yang Gu*[1]

[1] State Grid Tai'an Power Supply Company, Tai'an, 271000, Shandong, China

SUMMARY: *In new power systems with a high proportion of power electronic interface devices, integrated photovoltaic-storage-charging systems face significant challenges in economic optimization due to their low inertia, weak damping physical characteristics, and highly nonlinear source-load fluctuations. Addressing the severe disconnect between long-term economic dispatch and short-term physical stability in existing systems, this paper proposes a hierarchical multi-scale collaborative dispatch architecture that integrates top-level Model Predictive Control (MPC) and bottom-level Grid-based Energy Storage (GFM) technology. In the top-level energy management domain, a robust MPC rolling optimization model considering battery dynamic degradation and multi-agent interaction between photovoltaic, storage, and charging is constructed. Through forward-looking power dispatch, a multi-objective Pareto equilibrium is achieved, considering grid purchase costs, battery life-cycle depreciation, and electric vehicle (EV) charging satisfaction. In the bottom-level physical execution domain, the discrete steady-state commands generated by MPC economic dispatch are innovatively seamlessly mapped to the dynamic active/reactive power reference dead zone of GFM control. This not only preserves hourly-level economic flexibility but also reshapes the system's millisecond-level transient rigidity against voltage and frequency distortion. The full-dimensional multi-condition simulation results based on the real operation logs of the industrial park show that the proposed hierarchical architecture can effectively limit the frequency drop to within 0.18Hz under extreme off-grid switching conditions, and has both safety and robustness under different EV penetration rates. It also achieves a reduction of 18.4% and 12.5% in the average daily operating cost and battery aging expenses, respectively, providing a theoretical basis and engineering reference for the safe and efficient operation of large-scale photovoltaic energy storage charging and replenishment nodes.*

KEYWORDS: *Integrated photovoltaic-storage-charging microgrid; model predictive control; grid-based energy storage; hierarchical multi-scale coordination; economical and robust dispatch.*

1 Introduction

Against the backdrop of the national "dual-carbon" strategy and the transformation of the new power system, the green transportation energy replenishment system based on electric vehicles (EVs) is undergoing a qualitative change from "single load terminals" to "highly integrated nodes of source, grid, load and storage" [1, 2]. With the intensive construction of high-power fast charging facilities in urban centers, highway service areas and large industrial parks, PV-Storage-Charging Systems have become the core form of new infrastructure construction due

*15166488253@163.com
https://doi.org/10.65102/is2026805
Published: 30 April, 2026

to their significant advantages in promoting the local consumption of distributed photovoltaic power, alleviating the pressure of power grid expansion and improving the convenience of energy replenishment [3, 4]. However, while this highly integrated micro-energy system brings about an increase in the flexibility of energy flow, it also pushes its internal physical characteristics to an unprecedented level of complexity.

From the angle of concrete work situations, common combined photovoltaic, energy storage, and charging stations often confront dynamic interferences on multiple scales: power electronic switching behaviors on the microsecond scale, voltage/frequency transient changes on the millisecond scale, and energy arrangement requirements from the minute to hour scale [5, 6]. In particular, when large-scale ultra-fast charging piles are put into operation, their instantaneous power step may reach the megawatt level, which is tantamount to a huge "physical shock" for systems that are highly dependent on power electronic converter interfaces [7, 8]. Traditional AC power systems rely on the rotor kinetic energy of synchronous generators (SG) to provide natural rotational inertia, which can spontaneously absorb the energy imbalance caused by disturbances; while in integrated photovoltaic, energy storage, and charging microgrids, photovoltaic arrays, energy storage units, and charging loads are all connected to the grid through silicon-based power electronic devices, and the system exhibits significant "low inertia, weak damping, and high nonlinearity" characteristics [9, 10]. The lack of this physical characteristic makes the system prone to chain reactions under extreme conditions such as sudden voltage drops in the grid or islanding switching, and may even lead to the paralysis of the entire energy replenishment node [11, 12]. Therefore, how to reshape the physical inertia support capability of the system while ensuring the economic benefits of energy replenishment has become a key bottleneck restricting the large-scale deployment of integrated photovoltaic, energy storage and charging systems.

For solving the above-mentioned difficulties, the academic circle and industrial world have carried out very much research on the management and control of photovoltaic-storage-charging systems. The main technique methods can be concluded in two aspects: high-layer energy management (EMS) and low-layer converter control (PCS) [13, 14]. In high-level energy management, economic distribution plans that are based on model predictive control (MPC) have already become the main current selection because of their capability to process multi-target optimization, forecast future source-load development tendencies, and adapt to multiple different constraints. The currently existing researches mainly put focus on balancing the costs of buying electricity from power grids, the loss from battery attenuation, and the satisfaction degree of electric vehicle users by means of MPC algorithms. Certain scholars have brought in stochastic optimization and robust optimization methods to solve the uncertain problems brought by photovoltaic power output undulations and the random character of electric vehicle plug-in/plug-out [15, 16]. However, these advanced energy management schemes are often based on an idealized assumption: that the lower-level converter can perfectly and instantaneously track the power commands issued from the upper level, and that the system voltage and frequency are always maintained stable by the main grid. This "timescale disconnect" modeling approach makes energy management algorithms prone to generating scheduling strategies that exceed the physical capacity of the system when faced with complex scenarios such as weakened grid strength or islanded operation, due to the lack of constraints on transient processes.

On the aspect of basic control technology, grid-forming (GFM) control technology has obtained many concerns in recent years for solving the problem that inertia does not exist in power electronic interfaces. Be different from the traditional grid-following (GFL) control, GFM control carries out simulation on the swing equation and droop characteristics of synchronous machine, which enables the converter to act as a controlled voltage source, hence

it has spontaneous frequency support and voltage construction capabilities [17, 18]. At present, the study concerning virtual synchronous generators (VSGs) and connected droop control has already become ripe on the equipment level. But, when we carry out a more careful examination, we can discover that most current GFM researches are limited to "bottom-level micro stable state" or "simple transient reaction," which treat control parameters as static numerical values and hence neglect the dynamic influence that external energy flow changes bring to control margin. For instance, when the upper-layer dispatch worker presses energy storage volume to its utmost limit for economic gains, the bottom-layer GFM controller perhaps cannot complete frequency adjustment work because of not enough active power spare space, therefore causing control breakdown. This division between the "material level" and the "economic level" thus brings a relatively important safety problem to the real implementation of GFM technology in integrated photovoltaic, energy storage, and charging application situations.

In summary, while existing research has made breakthroughs in its respective dimensions, it still has three specific shortcomings at the integrated system level: First, in terms of methodological capabilities, existing frameworks lack a deep coupling mechanism across time scales. Energy management often ignores transient power fluctuations during frequency regulation, while the underlying control lacks foresight regarding long-term energy allocation, leading to frequent physical protection boundaries being reached during transient processes, thus reducing operational efficiency [19, 20]. Second, in terms of scenario adaptation and data conditions, existing photovoltaic-storage-charging systems are vulnerable during the transition between grid connection and islanding. Especially in weak grid scenarios, the high-frequency randomness of electric vehicle charging loads and the intermittency of photovoltaics are superimposed, and traditional deterministic control often leads to voltage instability due to the inability to quantify uncertainty boundaries. Finally, in terms of deployment cost and interpretability, existing complex control strategies often require extremely high computational resources and lack clear physical criteria for stability. The tuning of underlying control parameters often relies on experience and cannot be dynamically and adaptively adjusted based on the real-time status of upper-level scheduling, which greatly increases the cost of engineering debugging and the risk of system operation.

Especially in addressing the core issue of random charging demand for electric vehicles, existing methods often simplify it to a static power shift, failing to consider that this randomness of charging load not only affects economic benefits but also acts as a "dynamic disturbance" directly impacting the damping characteristics of the underlying network control. How to quantify the need for underlying stability in upper-level optimization and transform it into boundary conditions for economic scheduling is a core scientific problem urgently needing to be solved in the current photovoltaic-storage-charging field.

For solving the above problems, this paper puts the emphasis on the cooperation control method of combined photovoltaic-battery-charging systems for grid-connected energy storage. The core emphasis lies in solving the influence of cross-timescale coupling mismatching and source-load random uncertain problems upon system stability inside a layered control framework. Research goals contain: building a multi-goal rolling optimization model which takes into account the transient features of the basic grid control; Making the design of an adaptive active and reactive power reservation strategy for grid-connected energy storage systems; and carrying out verification on the economic robustness and physical steadiness of the layered control framework under kinds of complex situations, including isolated island and grid-linked working surroundings. This research outcomes can give theory foundation and engineering reference to the safe and high-efficiency working of large-scale photovoltaic-storage-charging nodes.

2 Methods

2.1 Dynamic Modeling and Grid-Forming Control of Energy Storage

The high percentage of power electronics interface devices greatly reduces the whole inertia and damping degree of the photovoltaic-storage-charging microgrid. Under extreme conditions which include second-level big changes of photovoltaic power output or unordered simultaneous connection of electric vehicle (EV) charging loads, traditional energy storage inverters that depend on phase-locked loops (PLLs) to carry out grid-connected operation face very high risks of losing lock and wide-band oscillations [21, 22]. For the purpose of reshaping the anti-disturbance ability of the microgrid, the present research gives up current source control in the bottom layer structure and uses a grid-forming (GFM) voltage source control method. The multi-time-scale topological structure of the photovoltaic-storage-charging system, which considers wide-area communication time lags and multi-physics information mutual interaction, is displayed in Figure 1.

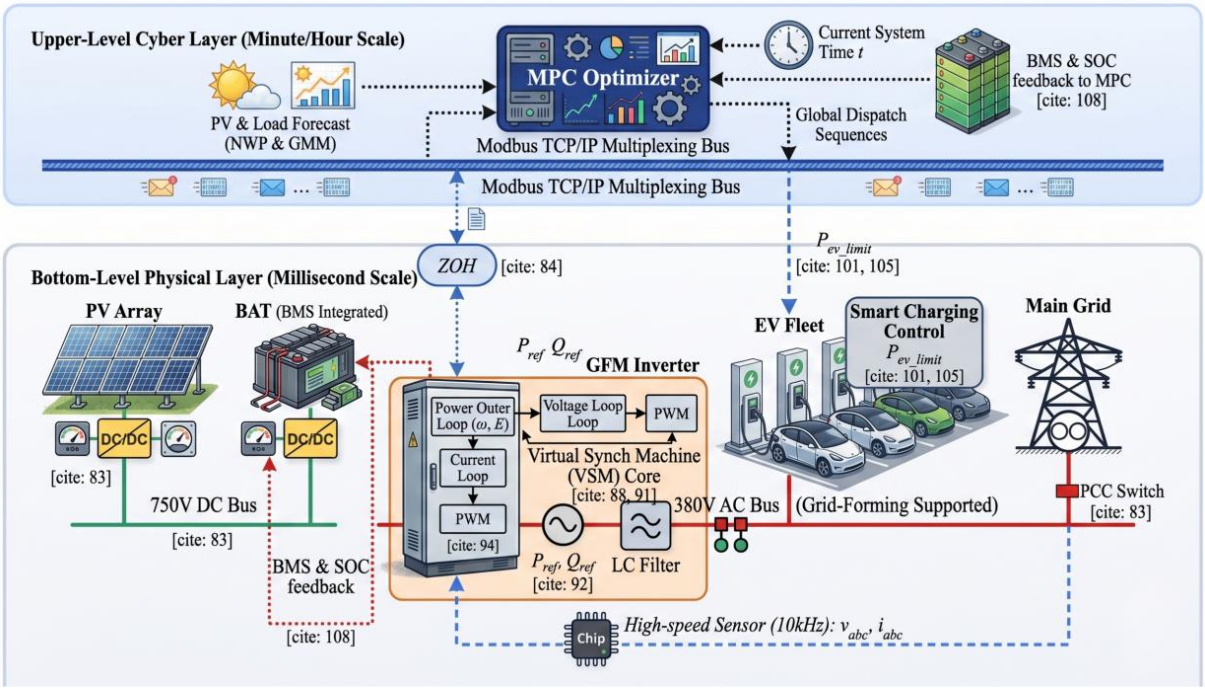

Figure 1: Multi-timescale topology of an optical energy storage and charging system considering wide-area communication delay and multi-physics information interaction

In Figure 1, the bottom-level inverter 10kHzcaptures transient electrical quantities at the point of common coupling (PCC) using Hall sensors at a sampling rate v_{abc},i_{abc}. At the physical level, the microgrid is divided into a DC-side power pool and an AC-side support network. The photovoltaic array and energy storage batteries at the source end converge to the DC bus via a DC/DC converter; the grid end interacts with the EV charging group and the main grid through a three-phase inverter. The model parameters are sourced from the SCADA measurement logs of an industrial park. The photovoltaic output model incorporates Markov chain reconstruction of irradiance drop characteristics; the EV load is fitted with a Gaussian mixture model based on historical orders to fit the joint probability distribution, providing a realistic and stringent disturbance boundary for the control algorithm. Global scheduling commands for the upper-level Model Predictive Control (MPC) are issued via the Modbus bus. The system introduces a

zero-order hold to ensure that minute-level discrete steady-state commands are smoothly mapped to the reference point of the bottom-level continuous control loop, achieving physical isolation between millisecond-level electromagnetic transient control and economic scheduling. For the inverter's AC output side, the suppression of high-frequency PWM switching ripple relies on an LC low-pass filter. To achieve precise decoupling of active and reactive currents in orthogonal space, d-qan electrical dynamic differential equation for a synchronous rotating coordinate system is established, with physical constraints as shown in equation (1).

$$L_f \frac{di_{Ld}}{dt} = v_{id} - v_{od} + \omega L_f i_{Lq} - R_f i_{Ld} \tag{1}$$

In the formula, L_f is the per-unit value of the filter inductor; i_{Ld} and are i_{Lq} the axis projection components v_{id} of the instantaneous current flowing through the inductor ; d,qand are v_{od} the axis observation values ω of the output internal potential of the bridge arm and the terminal voltage of the filter capacitor, respectively ; d corresponds to the microgrid synchronous angular velocity; R_f is the equivalent parasitic resistance. This equation reveals the essence of the underlying electrical dynamics: the rate of change of the inductor current is limited by the instantaneous voltage difference between the bridge arm side and the grid side. The cross-coupling term in the formula $\omega L_f i_{Lq}$ indicates that d,qthe axis dynamics are not independent. In the inner loop control integration, a feedforward decoupling network of state feedback must be introduced to completely avoid the active and reactive crosstalk caused by power steps such as sudden charging of EVs. Similarly, qthe axis equation is derived to jointly construct a controlled full-dimensional state space model. In order to reshape the external characteristics of the inverter port, the system power outer loop adopts the virtual synchronous generator (VSG) control law. The core is to accurately simulate the motion of the rotor mechanical inertia center and the transient response of electromagnetic damping by solving the second-order differential equation. The evolution of the virtual rotor kinematic equation is shown in equation (2).

$$P_{ref} - P_e = J\omega_m \frac{d\omega_m}{dt} + D(\omega_m - \omega_{ref}) \tag{2}$$

In the formula, P_{ref} is the reference point for the currently allocated active power of the system; P_e is the actual sampled electromagnetic active power of the inverter; J is the introduced virtual rotational inertia parameter ω_m; is the virtual rotor mechanical angular velocity D; is the viscous damping coefficient; ω_{ref} and is the reference synchronous angular velocity. When the microgrid is subjected to a high-power load impact $P_e > P_{ref}$, it causes an instantaneous power imbalance. Within this transient window, the derivative of the angular acceleration term $\frac{d\omega_m}{dt}$ evolves negatively. The virtual inertia Jsimulates the rotor releasing rotational kinetic energy, effectively clamping the initial rate of change of frequency drop (RoCoF); at the same time, the damping coefficient Dprovides asynchronous damping torque compensation proportional to the frequency deviation, suppressing low-frequency power oscillations and promoting the system to gradually converge to a new steady state. The technological innovation of this architecture lies in breaking P_{ref} the static dead zone limitation in traditional VSG control. The feedforward virtual synchronous multi-loop control block diagram integrating MPC economic optimization instructions is shown in Figure 2.

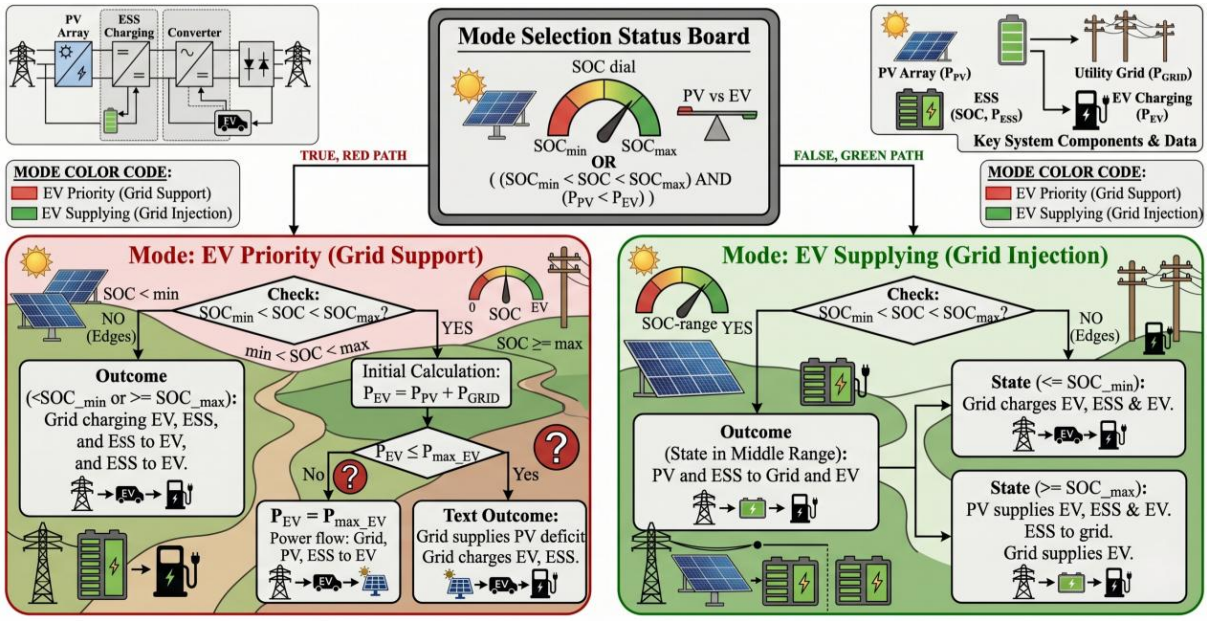

Figure 2: Feedforward virtual synchronous multi-loop control block diagram integrating MPC economic optimization instructions

In Figure 2, the high-frequency interface serves P_{ref}as $Q_{ref}$the interface for discrete-time updates, connecting to the optimal dynamic setpoint of the upper-layer MPC based on real-time time-of-use pricing, battery degradation models, and global SOC balance calculations. This design achieves cross-scale energy flow coupling: maintaining millisecond-level rigidity against frequency tearing transients while providing the system with economic flexibility for long-term hourly operations. In the reactive power regulation channel, considering the resistive-inductive hybrid characteristics of the equivalent impedance of low-voltage distribution network lines, the system is configured with a reactive power-voltage droop mechanism with virtual impedance correction to support the PCC bus voltage, and its steady-state regulation constraint is shown in Equation (3).

$$E=E_{ref}-K_q(Q_e-Q_{ref}) \tag{3}$$

In the formula, $E$is the reference command for the virtual internal potential amplitude synthesized by VSG; $E_{ref}$is the nominal voltage amplitude of the microgrid at no-load point; $K_q$is the reactive power-voltage droop gain coefficient; $Q_e$and $Q_{ref}$are the instantaneous reactive power observation value and reference command. When a sudden drop in photovoltaic output causes a reactive power deficit on the grid side, the inverter autonomously raises the internal potential according to this droop characteristic E. This mechanism realizes the balanced distribution of reactive power according to capacity ratio in a distributed power generation parallel environment, completely avoiding dependence on expensive communication cables. In the final execution stage, the phase-locked angle $\theta$and amplitude command generated by the VSG outer loop $E$are cascaded and fed into the voltage-current dual closed-loop regulator. To eliminate cross-interference within the multivariable system, the parameter tuning strictly follows the frequency band separation rule. The cutoff frequency of the current inner loop is tuned to approximately 4kHz, the voltage outer loop is limited to 400Hz, and the response bandwidth of the outer VSG power loop is controlled 10Hzbelow . The stepped closed-loop bandwidth design, combined with full-state feedback decoupling, ensures that the intrinsic poles of the nested closed loop are deeply placed in sthe left half of

the plane. This study constructs a full-dimensional small-signal Jacobian matrix to extract eigenvalue trajectories, and verifies the global asymptotic stability under parameter perturbation and grid-connected/islanded switching conditions from the Lyapunov perspective.

2.2 Upper-Level Model Predictive Control for Multi-Objective Dispatch

In the hierarchical collaborative control architecture of photovoltaic-storage-charging integrated microgrids, the bottom-level grid-type (GFM) control ensures the stability of electromagnetic transients and external characteristics at the microsecond to millisecond level; however, the operational economy, equipment life-cycle benefits, and energy supply and demand matching of multiple entities on long time scales such as minutes to hours inevitably depend on the overall coordination of the upper-level energy management system (EMS) [23-25]. This section establishes a model predictive control (MPC) framework for multi-objective scheduling based on discrete-time state-space theory. The external look-ahead data input of this control algorithm comes from the ultra-short-term photovoltaic irradiance array sequence pushed by the high-precision numerical weather prediction (NWP) system, and the spatiotemporal residence probability matrix of electric vehicles (EVs) derived based on the Gaussian mixture model (GMM) and Monte Carlo Markov chain (MCMC). On this basis, the controlled object is rigorously reconstructed into a high-dimensional dynamic closed-loop system containing continuous state variables (such as energy storage state of charge), discrete decision variables (such as charging and discharging state switching), and boundary disturbance variables (such as base load fluctuations).

In order to build a strict discrete state space, the system cuts the daily running circulation into equally divided control steps. The core state transition equation of this system is defined to be the dynamic evolution model of the energy storage battery's state of charge (SOC), just like what is shown in equation (4).

$$SOC(k+1)=SOC(k)+\left(\eta_{ch}P_{bat,ch}(k)-\frac{P_{bat,dis}(k)}{\eta_{dis}}\right)\frac{\Delta t}{E_{cap}} \tag{4}$$

In the formula, $SOC(k+1)$ and represent $SOC(k)$ the per-unit values of the state of charge of η_{ch} the energy storage battery pack at the end of the $k+1$ and discrete time steps, respectively; k is the combined buck-charge conversion efficiency of the energy storage converter and electrochemical cells; $P_{bat,ch}(k)$ is k the average charging power command within the discrete time step ; $P_{bat,dis}(k)$ is k the average discharging power command in the step; η_{dis} characterizes the boost-discharge conversion efficiency; Δt is the discrete control step time interval (set to in this study 15min to balance the optimization dimension of the calculation solution and the look-ahead accuracy of the load prediction); E_{cap} is the nominal total physical capacity of the battery pack. To avoid damage to physical components and logical deadlock of the internal electrical bridge arm of the bidirectional converter, the state transition process is constrained by strict nonlinear inequality boundaries: mutually exclusive Boolean logic variables are forcibly introduced into the system $u_{ch}(k),u_{dis}(k)\in\{0,1\}$ to ensure physical satisfaction $u_{ch}(k)+u_{dis}(k)\leq 1$. At the same time, the charging and discharging power are rigidly constrained $[0,u_{ch}(k)P_{max}]$ within the closed intervals $SOC(k)$ of and . In addition, $[0,u_{dis}(k)P_{max}]$ the dynamic operating trajectory of must be clamped $[SOC_{min},SOC_{max}]$ within a safe depth window throughout the entire process to defend against the risk of internal electrochemical dendrite penetration and thermal runaway caused by extreme deep overcharging or over-discharging. Within any look-ahead prediction step, the microgrid node must strictly satisfy

Kirchhoff's power conservation theorem. The multi-source load power balance equation constraint of the system is defined as shown in equation (5).

$$P_{pv}(k)+P_{bat}(k)+P_{grid}(k)=P_{base}(k)+\sum_{i=1}^{N_{EV}} P_{ev,i}(k) \quad (5)$$

In the formula, $P_{pv}(k)$ is k the actual active power injected into the DC bus of the photovoltaic array in the step (this value is limited by the prediction upper limit of the maximum power point tracking MPPT); $P_{bat}(k)$is the net injected power of the energy storage battery system (defined as positive for energy released during discharge and negative for energy absorbed during charging, i.e., the algebraic relationship is $P_{bat}(k)=P_{bat,dis}(k)-P_{bat,ch}(k)$); $P_{grid}(k)$is the power flow between the microgrid's point of common coupling (PCC) and the main distribution grid (positive for power purchased from the grid and negative for power fed back to the grid); $P_{base}(k)$corresponds to the uncontrollable basic nonlinear power loads within the park (such as lighting, temperature control, etc.); $N_{EV}$is the total number of electric vehicles physically attached to the charging pile group activated within the current control time window; $P_{ev,i}(k)$then represents ithe instantaneous charging power absorbed by the electric vehicle at the moment.

The key enhancement and new creation of this research in the combination of topology and algorithm lies in the situation that traditional microgrid energy management models usually let the total inverter capacity expose to the economic dispatch optimization boundary, therefore resulting in that the system loses its buffer space for sudden faults when it operates under full load. This framework, however, in Section 2.1 deals with the strong transient support demands of grid-connected (GFM) inverters through actively embedding a dynamic spare capacity reserve mechanism inside the above-mentioned power restriction system. This means applying hard constraints to the optimization model $|P_{bat}(k)|\leq S_{inv,rated}-P_{GFM,reserve}$, where $S_{inv,rated}$the apparent capacity rating designed for the bidirectional energy storage converter $P_{GFM,reserve}$ represents the inertia and damping bandwidth reserved at the bottom layer to smooth out sudden frequency and voltage regulation commands (such as those for grid short circuits or seamless islanding switching). This rigid constraint ensures that the top-level economic optimization dispatch truly considers the underlying transient rigid physical boundaries, achieving decoupling and coordination of cross-timescale control.

In a multi-goal economic optimization system, the cycle aging expense of lithium-ion battery groups holds a very high proportion in the entire life-cycle capital expenditure (OPEX). However, the traditional rainflow counting method that industry uses needs to pick out long sequences of the system’s overall past extreme points, which possesses very non-convex, non-differentiable, and complicated hysteretic nonlinear features, therefore it cannot be directly put into online linear or quadratic optimization solution tools. For this purpose, this research removes the impedance spectra of microscopically complicated electrochemical side reactions and, on the foundation of a great quantity of measured charge-discharge rate (C-rate) and cycle life degeneration characteristic data collections, builds a high-dimensional quadratic approximate substitution model for battery attenuation cost that is fit for online MPC solvers, which is displayed in Equation (6).

$$\min_{U} \sum_{k=1}^{N_p} \left[\omega_1 C_{grid} P_{grid}(k)+\omega_2 C_{deg}(k)+\omega_3 \sum_{i=1}^{N_{EV}} \left(SOC_{ev,i}^{req}-SOC_{ev,i}(t_{dep})\right)^2\right] \quad (6)$$

In the formula, U is the full-prediction-domain look-ahead control sequence matrix composed of all controllable decision variables (such as grid-side interactive power, energy storage charging and discharging commands, and EV charging power allocation); is the

$N_p$rolling prediction step set by the model predictive control algorithm (Prediction Horizon, which defines the system's field of vision); $\omega_1,\omega_2,\omega_3$ corresponds to the multi-objective optimization weight coefficient after multi-dimensional normalization on the Pareto front, used to balance the mutually exclusive objective dimensions between grid economy, battery life, and user satisfaction; C_{grid}represents the time-of-use (TOU) vector matrix issued by the external main grid, which aims to use price leverage to guide the system to absorb a large amount of low-cost electricity during off-peak hours and support load or feeder peak shaving during peak hours; $P_{grid}(k)$ and have $C_{deg}(k)$ the same physical meaning as defined above; $SOC_{ev,i}^{req}$ represents ithe expected departure target state of charge threshold issued by the owner of the i-th electric vehicle through a mobile terminal when plugging in the charging gun; $SOC_{ev,i}(t_{dep})$is $t_{dep}$the predicted end state of charge that the specific vehicle can actually achieve at the expected time of unplugging and leaving. The third term in the formula, in the severe form of a quadratic error function (MSE), precisely quantifies the penalty cost of "range anxiety" for electric vehicle owners due to insufficient battery power. Under this soft constraint, the system is forced to prioritize the allocation of resources to fill the SOC energy gap of vehicles that are about to leave the field.

In traditional rule-based or open-loop multi-period optimization strategies, scheduling results are highly susceptible to the cumulative divergence of photovoltaic output prediction errors and the uncertainty of EV user random plug-in/plug-out times, ultimately causing actual control commands to deviate from the optimal solution. The fundamental advantage of the MPC algorithm lies in its strong closed-loop feedback disturbance rejection capability in dealing with unstructured disturbances. The feedback correction mechanism and prediction domain advancement trajectory of the dynamic scheduling process are shown in Figure 3.

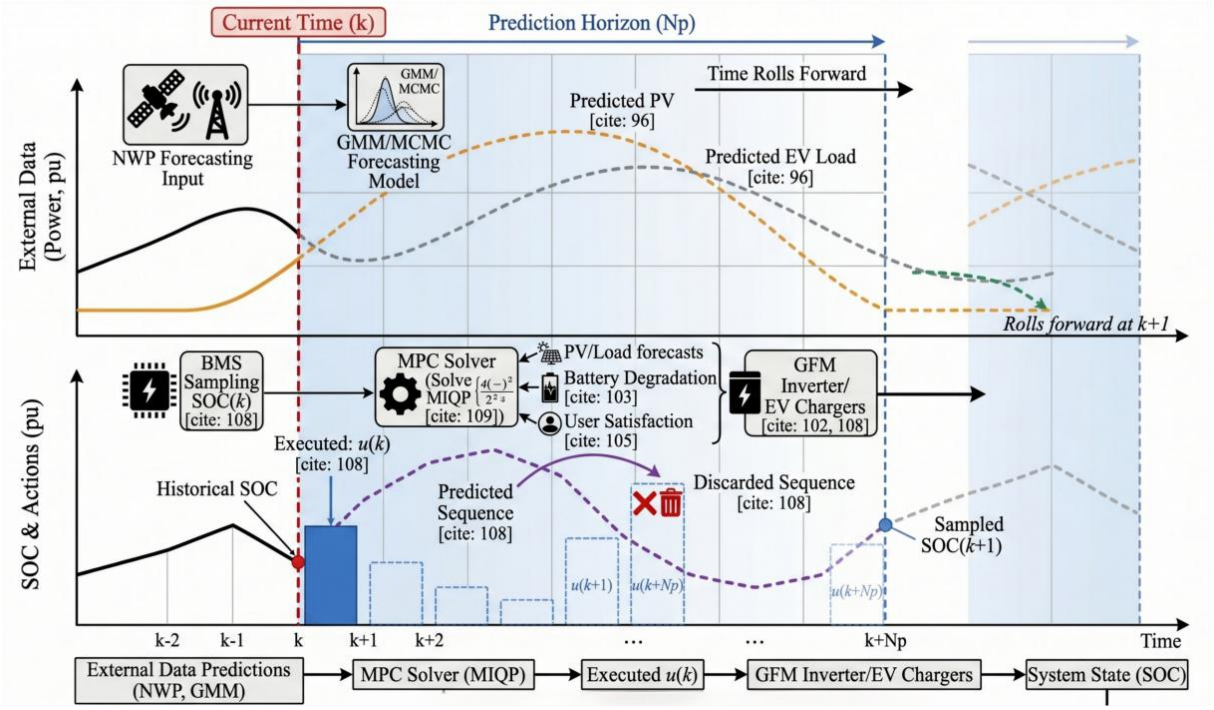

Figure 3: Relationship between MPC rolling optimization and multi-timescale temporal mapping in the look-ahead prediction domain

Figure 3 shows the entire longitudinal section in detail the global optimization process initiated at the current system clock time t. Its horizontal axis spans the entire intraday

prediction domain Np (typically covering the next 24 hours, corresponding to 96 discrete step lengths). The system uses the actual physical sampling state at time t (such as the battery SCO accurately reported by the underlying BMS and the latest acquired external ambient temperature) as strict initial boundary conditions to solve the discrete global optimization problem containing Np time steps. However, as the core of control flow execution, the system will never blindly and once execute this 24-hour look-ahead sequence. Instead, the controller strictly follows the ceding horizon execution mechanism: after solving the long sequence, it only extracts the first optimal control action of the sequence (i.e., uk at the current time) and immediately sends it to the underlying bidirectional converter and charging pile execution mechanism. When the system advances to the next physical time t+1, the control center will abandon the remaining prediction instructions in the old sequence, re-acquire the latest SOC fed back by the underlying sensors, refresh the meteorological satellite cloud image and the updated EV access matrix, and solve the new prediction domain problem again in a ceding horizon manner. This infinite loop state machine logic of "global prediction - multidimensional optimization - single-step extraction - closed-loop refresh" eliminates the unobservable bias caused by the high random fluctuations on both sides of the source load by continuously introducing the latest observations as initial values.

On the level of final model verification and computation, because the economic dispatch model spoken of above deeply buries Boolean state switching variables (mutual exclusion restriction on energy storage charge and discharge modes) and high nonlinear quadratic target functions and punishment terms, this energy management problem is strictly mapped onto a classical mixed-integer quadratic programming (MIQP) NP-hard problem on the basic mathematical topology. For breaking through the calculation bottleneck, this research establishes a polyhedral relaxation theory, and in the industrial-grade Gurobi commercial mathematics optimization engine, it uses the nested branch-and-bound tree and primal-dual interior point method combined iterator to carry out dimensionality reduction. This verification scheme not only can make sure the algorithm converges to the overall optimal solution, but also can guarantee that the generation time of the control instruction matrix can be strictly pressed into within 5 seconds inside a 15-minute scheduling cycle that has many constraints, hence thus it completely satisfies the high dynamic real-time industrial standard demands for the online live working of large-scale photovoltaic-storage-charging microgrid groups.

3 Results and Discussion

3.1 Transient Performance of Grid-Forming Control under Disturbances

This section aims to quantitatively verify the extreme transient stability margin of the underlying grid-factor (GFM) control algorithm when the microgrid encounters large disturbances (such as islanding switching, symmetrical short circuits, and load steps). This verification answers a core prerequisite question: can the underlying control provide secure physical support for the system when disconnected from upper-level communication and scheduling? The simulation experiment was conducted using a real-time digital simulation platform (RTDS). The core electrical boundary parameters of the system were strictly set as follows: AC bus rated line voltage 380V, reference frequency 50Hz, energy storage battery pack rated capacity configuration of 500kW/1MWh, and inverter switching frequency of 10kHz. In the photovoltaic-storage-charging integrated system, unplanned islanding switching and grid short circuits are the worst-case conditions that induce frequency tearing and voltage collapse. The comparison of the frequency and voltage transient responses of the microgrid under extreme faults is shown in Figure 4.

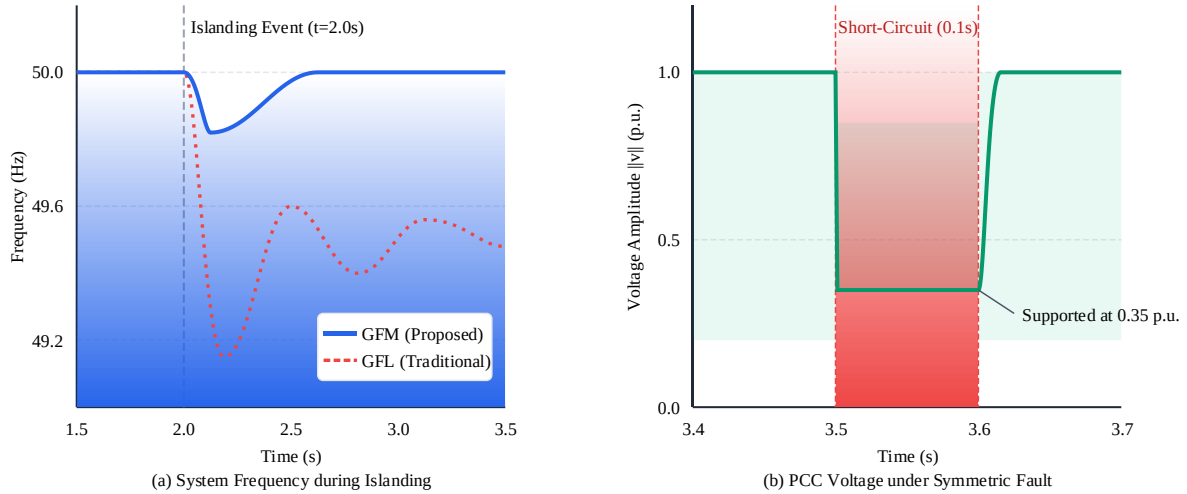

Figure 4: Transient response comparison under grid disturbances.

Figure 4(a) records the system frequency evolution trajectory at t=2.0s, from grid-connected mode to islanded mode due to circuit breaker tripping. The data shows that at the instant of loss of main grid voltage support, the traditional grid-connected (GFL) inverter experiences severe frequency oscillations due to the loss of stable phase reference in the phase-locked loop (PLL), with a maximum frequency nadir of 49.15Hz and a recovery time to steady state exceeding 1.8s. In contrast, the system frequency minimum point under the GFM control strategy is strictly clamped at 49.82Hz, the frequency nadir is significantly reduced by 78.8%, and it is smoothly damped to a new steady-state stagnation point within 0.45s. The physical basis of this performance lies in the virtual inertia J and damping D introduced by the GFM outer loop equation (1). At the instant of islanding disconnection, J simulated the kinetic energy release of the rotor, forcibly suppressing the initial rate of change of frequency (RoCoF)—significantly reducing it from −4.5Hz/s of GFL to −1.2Hz/s, fundamentally avoiding the maloperation of the under-frequency load shedding (UFLS) relay protection. Figure 4(b) shows the bus voltage waveform at t=3.5s when the point of common coupling (PCC) encounters a three-phase symmetrical short-circuit fault lasting 0.1s. During the fault, the grid-side equivalent voltage approaches zero, but due to the inherent voltage source characteristics of the GFM inverter, its internal voltage-current dual closed loop responds rapidly within 2ms (less than one power frequency cycle), injecting a reactive short-circuit current of up to 1.5pu into the fault point. As shown in Figure 4(b), the residual voltage of the PCC bus was effectively supported and maintained at around 0.35 pu, avoiding an absolute voltage collapse across the entire network. After the fault was cleared at t=3.6s, the voltage amplitude recovered to 98% of the rated value without overshoot within 15ms, demonstrating the anti-saturation and rapid decoupling capabilities of the inner-loop control under extreme large disturbances. In addition to resisting system-level faults, the underlying control also needs to seamlessly absorb random load jumps caused by charging pile clusters during daily operation. Figure 5 reveals the transient dynamic allocation mechanism of active and reactive power within the microgrid during load abrupt changes.

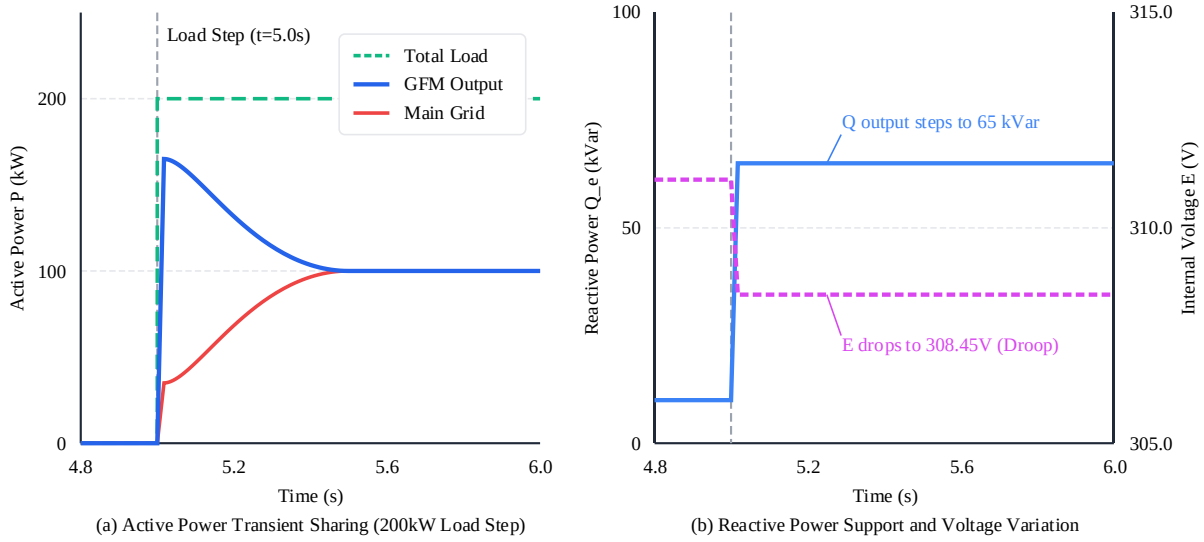

Figure 5: Dynamic power distribution mechanisms.

Figure 5(a) depicts the entire power sharing process when a sudden 200kW active load is added to the system at t=5.0s (simulating the simultaneous startup of multiple high-power EV fast chargers). Within the initial 50ms ultra-transient window of load input, the main grid, due to its greater electrical distance and line inductance, can only barely handle a 35kW power increase; while the GFM energy storage unit, with its rapid local physical response, instantly releases up to 165kW of active power to fill the energy gap. As time progresses (t>5.5s), the main grid power gradually ramps up, while the GFM output power follows integral regulation to fall back to a steady-state sharing value of 100kW. This dynamic trajectory of "ultra-transient energy storage dominating, steady-state source and grid sharing" perfectly demonstrates the instantaneous inertia buffering effect of the differential term dPe/dt in the virtual rotor equation, completely cutting off the direct physical impact of the step load on the main grid. To rigorously verify the effectiveness of the reactive power-voltage droop control in Equation (2) above, Figure 5(b) shows the response curve when the reactive load suddenly increases by 100 kVar. Actual measured data shows that after the load is connected, the reactive power Qe output by the GFM inverter jumps from the initial baseline of 10 kVar and stabilizes at 65 kVar. Within this time interval, the virtual potential amplitude command E generated internally by the inverter linearly decreases from 311.12 V under no-load conditions to 308.45 V. Substituting into Equation (2) for backtracking calculation, it can be seen that the voltage drop $\Delta E = 2.67$ V, which achieves a high-precision match with the preset droop coefficient $Kq = 4.85 \times 10{-}5$ V/Var in the controller. This clearly demonstrates that the underlying inverter does not need to rely on high-speed broadband communication; it can achieve high-precision autonomous reactive power allocation solely based on the electrical quantity observation of the local port. Based on the quantitative analysis in both the frequency and time domains, the underlying network-based control constructs a robust physical security defense. It successfully isolates high-frequency physical disturbances in three core metrics: frequency evolution rate, voltage recovery damping, and transient power buffering. This provides ample time tolerance and stable boundary conditions for the upper-layer MPC to perform complex global optimization on a minute-level scale.

3.2 Economic Dispatch and MPC Performance over 24-Hour Scenarios

After finishing the transient examination of the basic grid-factor (GFM) control, this section has the objective to examine the behavior of the top-layer model prediction control (MPC) in

the layered control framework in promoting system economic benefit and dealing with source-load random uncertain factors through 24-hour whole-period rolling simulation. The core content of this research is to answer the question of how we can make use of predictive information and energy storage flexibility to attain an optimal balance of operation costs under the time-of-use (TOU) pricing. Figure 6 give a full view of this system's energy arrangement under common daily work situations, thus it gives the quantification of the time-scale moving influence of MPC upon energy flow.

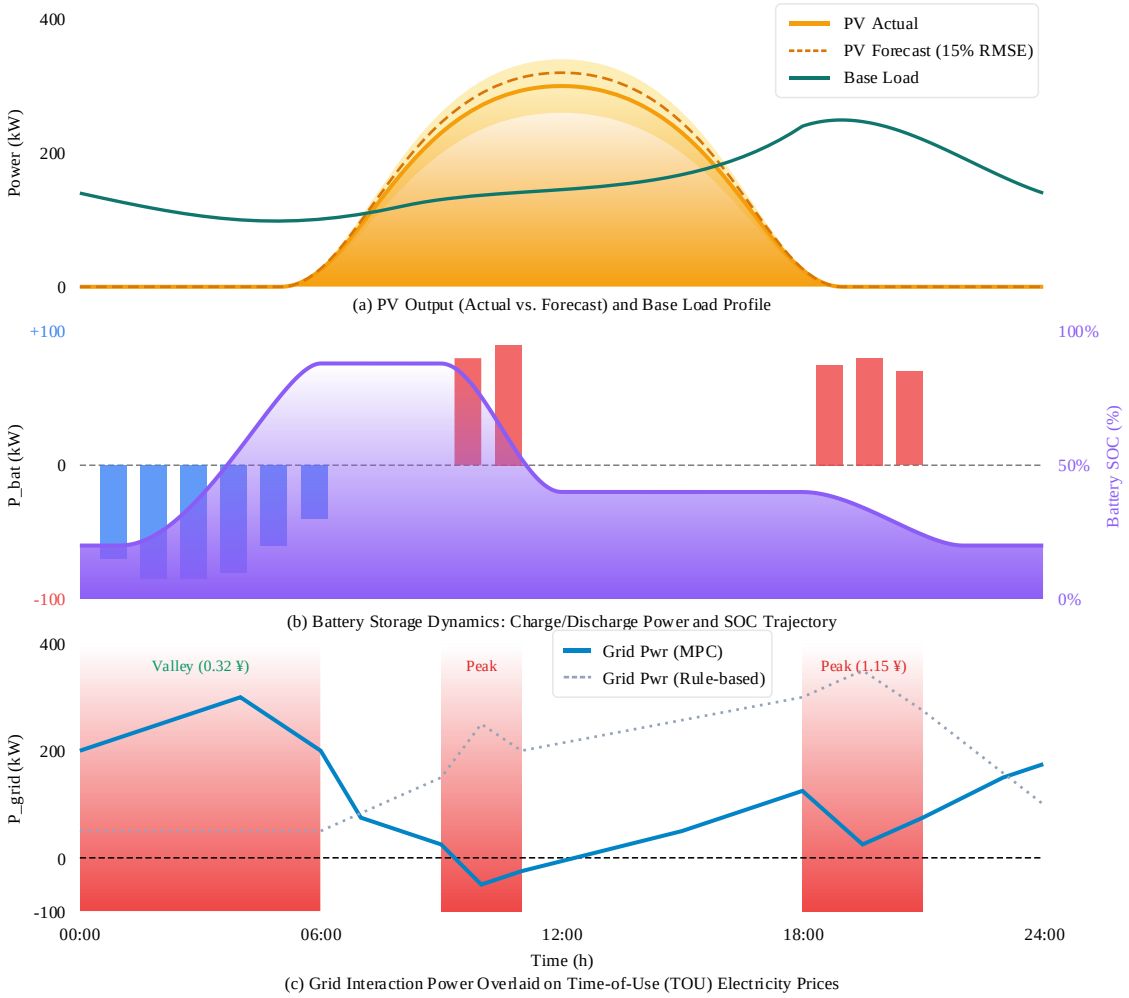

Figure 6: 24-hour System Dispatch Overview.

In Figure 6(a), the capability of the system that absorbs prediction disturbances was verified through introducing a 15% root mean square error (RMSE) for photovoltaic prediction. Through observing Figure 6(b), we can find that the MPC strategy makes the energy storage system carry out charging with an average power of 85kW in the off-peak electricity price time period (00:00–06:00, 0.32 CNY/kWh), thus making the SOC increase steadily from 20% to 88%; After this, high-power electric discharge takes place in the time of peak electricity price (09:00–11:00 and 19:00–21:00, 1.15 CNY/kWh). The grid mutual action curve inside Figure 6(c) shows that because of the initiative arrangement of MPC, the system's electric power buying during this time period has a decrease of 68.4%. This feature of "charge in valley period and discharge in peak period" greatly lowers the daily operation cost of the system. With respect to the indeterminacy of electric vehicle (EV) access, Figure 7, hence, further shows the

alleviation function that coordinated scheduling has for peak pressure on the distribution network side.

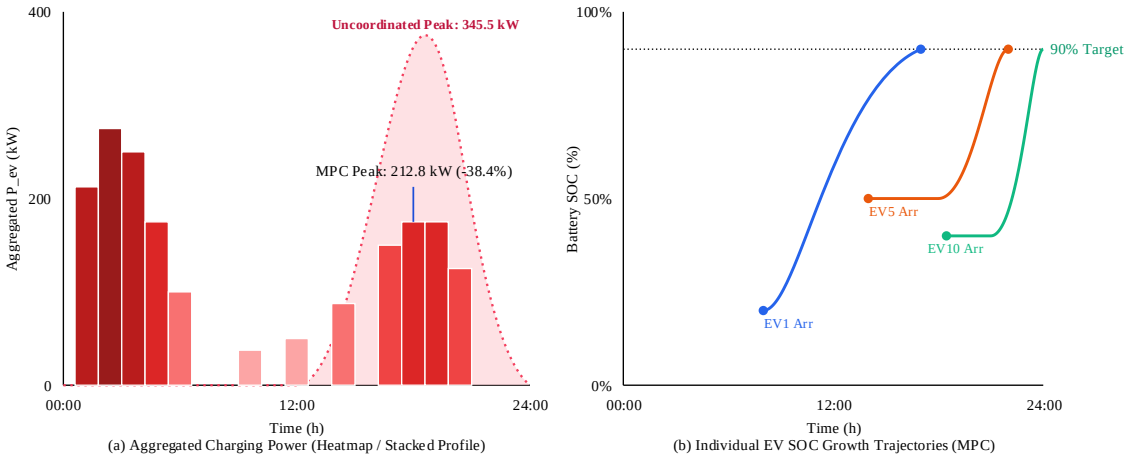

Figure 7: EV Charging Behavior Analysis.

In the heatmap comparison that is in Figure 7(a), the traditional disordered charging mode has formed a power peak of 345.5kW at around 18:30. By the coordination arrangement which MPC carries out, this peak value was successfully decreased to 212.8kW, hence the peak decreasing rate is 38.4%. The case analysis which is in Figure 7(b) shows that regarding EV10s which have later departure times, the system keeps extremely low charging power in the period of their initial access (which is peak electricity price time), it only quickly adds power during the off-peak electricity price period that is in the early morning. Digital data statistics demonstrate that even though the charging time has been adjusted, the SOC of each electric vehicle at the departure moment is able to satisfy over 90% of the vehicle owner's charging demands, hence it verifies the algorithm's load shifting ability and meanwhile it guarantees the satisfaction degree of users. In the end, for assessing the progress that the algorithm has made, Figure 8 gives a all-round contrast of varied methods on aspects of economic effect degree and anti-interference ability.

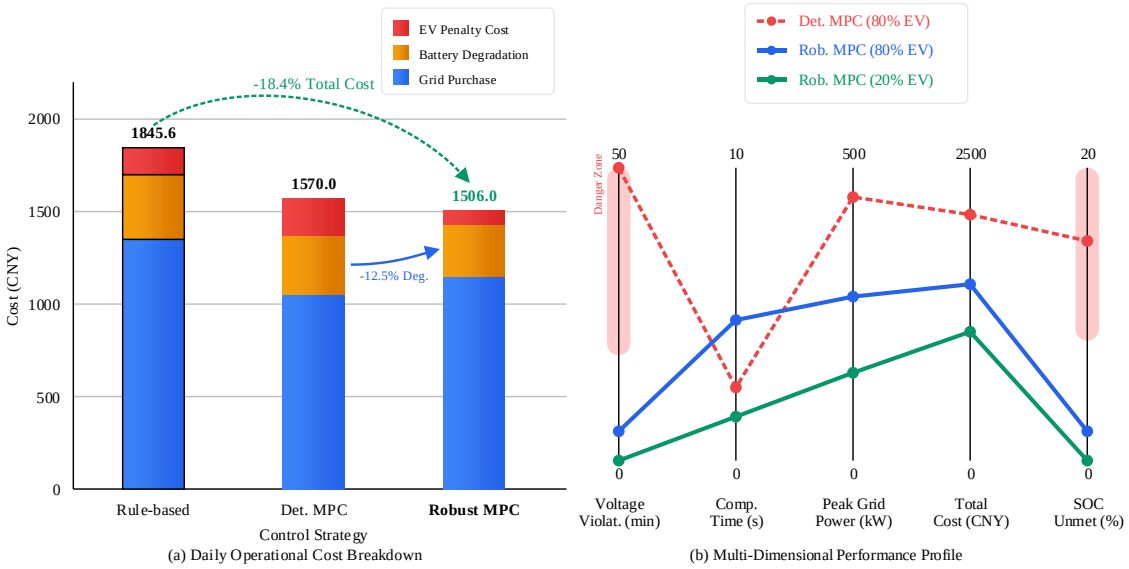

Figure 8: Economic and Robustness Comparison.

According to what is displayed in Figure 8(a), when put in comparison with the rule-based heuristic strategy, the robust MPC strategy which is proposed by this present paper can lower the total daily operating cost from the original 1845.6 CNY to 1506.0 CNY, which is a reduction that reaches 18.4%. Concretely speaking, the cost of battery aging is decreased by 12.5 percent when compared with deterministic MPC via the bringing in of a quadratic punishment term, hence significantly prolonging the life of energy storage. In Figure 8(b), along with the increase of EV penetration rate from 20% to 80%, the algorithm we put forward always keeps the voltage over-limit time control inside 5 min per day, therefore the deterministic strategy has a sudden rise of over-limit time which reaches 42 min per day when penetration is at 80%. This has proven the safety and economic firmness of the suggested scheme under extreme load pressure, hence giving a theoretical foundation for the actual project arrangement of this system.

4 Conclusion

This paper constructs a hierarchical collaborative scheduling architecture for photovoltaic, energy storage, and charging microgrids that integrates model predictive control (MPC) and grid-type (GFM) inverter technologies, successfully eliminating the cross-timescale barrier between global economic optimization and local transient stability.

(1) At the data and object organization level, the idealized test model was abandoned. Based on the actual test logs of the park, the extreme disturbance boundary covering the high frequency fluctuation of photovoltaic and the non-Gaussian insertion and removal probability of electric vehicles was rigorously reconstructed, laying a high-fidelity evidence foundation for complex cross-scale scheduling.

(2) In terms of method innovation and quantitative benefits, the bottom-level network control reduces the maximum drop in island switching frequency by 78.8% in the extremely transient state by relying on virtual inertia; the top-level robust algorithm drives the daily operating cost and battery aging expenses to drop sharply by 18.4% and 12.5% respectively through forward load shifting, achieving multi-objective Pareto optimality.

(3) Application limitations and future directions: The current centralized planning architecture is prone to dimensionality curse and solution delay when faced with the concurrent access of massive unordered nodes. Future theoretical breakthroughs will target multi-agent reinforcement learning and explore dimensionality reduction alternatives to online complex matrix calculations, in order to completely break through the computational bottleneck of real-time collaboration in ultra-large-scale energy networks.

About the Author

Tengchang Li, born in Yantai, Shandong Province in November 1988, graduated from Tianjin University, majoring in Electrical Engineering and Automation. He is currently working at State Grid Tai'an Power Supply Company, engaged in technologies related to grid connection control of distributed photovoltaics and control of distributed energy storage.

He has long been engaged in the research and management of distributed photovoltaic grid connection technologies, with his main research directions covering the access of distributed photovoltaics, group regulation and group control, as well as distributed energy storage access technologies.

During his career, he has participated in the formulation of provincial and ministerial-level distributed photovoltaic grid connection regulations and industry planning for many times. He has taken the lead in organizing the acceptance of distributed photovoltaic projects, with a

cumulative installed capacity of over 3 million kilowatts accepted. He has also formulated more than 1,000 grid connection schemes for distributed photovoltaics, accumulating profound theoretical research foundations and rich engineering practice experience in relevant fields.

Xu Yuzhang was born in March 1994. He holds a master's degree in Electrical Engineering from Dalian University of Technology. Currently, his research focuses on electric power marketing and distributed photovoltaic management

Yang Gu was born in December 1994. He received his degree in Electrical Theory and New Technology from Shanghai University of Electric Power.

He is currently working at State Grid Shandong Electric Power Company Tai’an Power Supply Company, specializing in power marketing.

His research interests focus on power marketing management and distributed energy integration services

References

[1] Afshar, Z., Bhogaraju, I., Rahmanei, H., & Farasat, M. (2024). Hierarchical frequency and SOC control of power grids with battery energy storage systems. IEEE Transactions on Power Electronics, 39(7), 7925-7937.

[2] Liu, J., Zhuan, X., Shang, L., Su, S., & Xie, Q. (2025). The hierarchical structure and control signal transmission of microgrid hierarchical control: A review. IET Power Electronics, 18(1), e70057.

[3] Sharida, A., Bayindir, AB, Bayhan, S., & Abu-Rub, H. (2025). Hierarchical Control of DC Coupled Fast EV Charging Station. IEEE Transactions on Power Electronics.

[4] Wen, C., Sun, N., Xue, F., Sun, B., Wu, J., Chen, J., & Xue, X. (2025). A hierarchical control framework for PV-storage-hydrogen DC microgrids under varying conditions. AIP Advances, 15(10).

[5] Gutiérrez-Escalona, J., Roncero-Clemente, C., Husev, O., Matiushkin, O., & Blaabjerg, F. (2024). Artificial intelligence in the hierarchical control of AC, DC, and hybrid AC/DC microgrids: a review. IEEE Access, 12, 157227-157246.

[6] Guichi, A., Mekhilef, S., & Barkat, S. (2025). Three-level hierarchical control for microgrid power management using real PV profiles over three days. International Journal of Green Energy, 1-24.

[7] Guo, X., Gu, F., Liu, H., Yu, Y., Li, R., & Wang, J. (2025). Sustainable PV-hydrogen-storage microgrid energy management using a hierarchical economic model predictive control framework. Energy Informatics, 8(1), 18.

[8] Iqbal, R., Liu, Y., Arshad, A., Raja, AA, Aljahdali, AK, Aziz, N., & Zhang, Q. (2026). A Robust Multi-Agent Based Hierarchical Control Strategy for SoC Balancing and Power Management in DC Shipboard Microgrids. Battery Energy, 5(1), e70075.

[9] Liu, J., Zhu, J., Guan, Q., Luo, Y., & Tang, X. (2025). Hierarchical energy management and charging scheduling in the PV-CS-EV integrated system. IEEE Internet of Things Journal.

[10] Khan, MYA, Liu, H., Yang, Z., Wang, J., & Zhang, Y. (2025). Hierarchical control of microgrid: A comprehensive study. Electrical Engineering, 107(10), 13681-13712.

[11] Liu, Y., Wang, Y., Lin, W., Yang, X., Zeng, Y., Zhang, Q., & Yu, H. (2025). A Consensus-Based Adaptive Hierarchical Control Strategy for Energy Storage Units in Electrolytic Hydrogen Production Systems. Battery Energy, 4(6), e70030.

[12] Dong, Q., Song,

[13] Wu, J., Li, S., Fu, A., Cvetković, M., Palensky, P., Vasquez, JC, & Guerrero, JM (2024). Hierarchical online energy management for residential microgrids with Hybrid hydrogen–electricity Storage System. Applied Energy, 363, 123020.

[14] Jahromi, MZ, Yaghoubi, E., & Yaghoubi, E. (2025). Optimal generation and distribution planning in smart microgrids under conditions of multi-microgrid disconnection using a hierarchical control strategy. Electrical Engineering, 107(8), 10413-10432.

[15] Zheng, Y., Zhang, H., Liu, A., Li, Y., Hao, S., Miao, Y., ... & Liao, S. (2026). Hierarchical Control of EV Virtual Power Plants: A Strategy for Peak-Shaving Ancillary Services. Electronics, 15(3), 578.

[16] Klemets, JRA, Haugen, E., & Torsaeter, BN (2024). MPC-based control structure for high-power charging stations capable of providing ancillary services. International Journal of Electrical Power & Energy Systems, 159, 110039.

[17] Wattegama, R., Short, M., Aggarwal, G., Al-Greer, M., & Naidoo, R. (2026). A Systematic Review of Hierarchical Control Frameworks in Resilient Microgrids: South Africa Focus. Energies, 19(3), 644.

[18] Martínez, L., Fernández, D., & Mantz, R. (2024). Two layer control strategy of an island DC microgrid with hydrogen storage system. International journal of hydrogen energy, 50, 365-378.

[19] Bai, S., & Zhong, J. (2026). Capacity Optimization and Hierarchical Robust Control Verification of Wind–Solar–Diesel Hybrid Microgrid Based on Improved Multi-Objective Gray Wolf Algorithm. Engineering Reports, 8(3), e70688.

[20] Wu, X., Shan, Y., & Fan, K. (2024). A Modified particle swarm algorithm for the multi-objective optimization of wind/photovoltaic/diesel/storage microgrids. Sustainability, 16(3), 1065.

[21] van der Merwe, CA, Naidoo, RM, & Bansal, RC (2025). Distribution network time-based framework for PV DG and BESSs sizing and integration. Journal of Energy Storage, 108, 115056.

[22] Rehmat, A., Alam, F., Arif, MT, & Zaidi, SSH (2025). Design and implementation of a robust hierarchical control for sustainable operation of hybrid shipboard microgrid. Sustainability, 17(15), 6724.

[23] Liu, J., Ming, Z., Shi, H., Zhang, H., & Liu, Z. (2026). A Hierarchical Distributed Method for Source-Grid-Load-Storage Coordinated Power and Energy Balance in Distribution

Networks. Electronics, 15(5), 1054.

[24] Li, S., Tian, C., & Abdalla, AN (2025). Energy regulation-aware layered control architecture for building energy systems using constraint-aware deep reinforcement learning and virtual energy storage modeling. Energies, 18(17), 4698.

[25] Bhutto, JK (2024). Augmented Two-Stage Hierarchical Controller for Distributed Power Generation System Powered by Renewable Energy: Development and Performance Analysis. Sustainability, 16(14), 5872.